Hindawi
International Journal of Aerospace Engineering
Volume 2023, Article ID 1215361, 12 pages
https://doi.org/10.1155/2023/1215361

Research Article

Nonlinear Predictive Control with Sliding Mode for Hypersonic Vehicle

Xiande Wu, Wenbin Bai, Yaen Xie, Qingnan Ma, and Xiangshuai Song

College of Aerospace and Civil Engineering, Harbin Engineering University, Harbin 150001, China

Correspondence should be addressed to Yaen Xie; xieenya@126.com

Received 13 January 2023; Revised 16 March 2023; Accepted 29 March 2023; Published 17 April 2023

Academic Editor: Chuang Liu

Hypersonic vehicles are difficult to control due to their rapid time variation, dynamic nonlinearity, strong coupling, and model uncertainty. This paper proposes a new nonlinear predictive controller to solve the problem. An improved model predictive controller is used to improve the dynamic control performance of hypersonic vehicles by converting nonlinear dynamics into a state-dependent linear model. The sliding surface can significantly increase the speed of convergence. The radial basis function is used to reduce the influence of system uncertainty. The stability of the proposed controller is analyzed based on the Lyapunov approach. The comparison of simulation results verifies the excellent control performance of the proposed method both in convergence speed and antidisturbance ability.

1. Introduction

Hypersonic vehicles are difficult to control due to their fast time variation, dynamic nonlinearity, strong coupling, and model uncertainty. The characteristics of the nonlinear dynamic model place high demands on the trajectory tracking control [1–4]. To ensure stable flight under complex constraints, the control system must have fast response and antidisturbance properties [3].

Many papers have been devoted to solving nonlinear control problems for hypersonic velocities, and many new controllers have been designed based on fault-tolerant control [5], robust control [6], adaptive control [7], predictive control [8], sliding mode control [9], and other control methods. The dynamic inverse controller is designed to actively compensate elastic disturbance and solve the system uncertainty problem [1, 4]. The robust controller is designed for height and velocity tracking control, and the nonlinear disturbance observer is used to estimate the external disturbances. These controllers can improve the robustness of the system [6, 7, 10]. Instruction filters and actuators are also used for robust nonlinear control to eliminate parameter uncertainty [3]. The adaptive tracking controller based on neural networks eliminates the uncertainty of the system [11].

Sliding mode control is a kind of nonlinear variable structure control, which has the advantages of fast response, strong antidisturbance ability, and strong robustness, and has been widely used in the control of hypersonic vehicle. [9] proposed a supertorsional sliding mode controller, which can approximate the global fast terminal sliding mode in finite time and is robust to uncertain parameters and other disturbances. In [12], a quasicontinuous sliding mode controller is designed based on the high-order sliding mode theory, which reduced the speed and height step response time and suppresses sliding mode chattering. For the problems of model parameter uncertainty and actuator failure, [13] uses a higher-order linearized model to establish an adaptive terminal sliding mode to eliminate chattering and establishes a fault-tolerant control system (FTC) to improve the fault-tolerant control capability of sliding mode control. The sliding mode controller based on power function is used to suppress its chattering effect, and the influence of disturbance on speed and height is suppressed through direct feedback [14].

[8, 15] have studied predictive control. The predictive control method has low requirements, good dynamic control

performance, and online rolling optimization calculation, which can better compensate the uncertainty caused by model mismatch, distortion, and disturbance. [16] proposed a new passive fault-tolerant control method based on weighted tubular MPC. By introducing weighting factors, the control performance of the system can be improved while the robustness of the system is sacrificed. [17] proposed a predictive control method based on the improved model and introduced an online parameter estimation method to eliminate the uncertainty and unknown interference of the dynamic model. [18] proposed a tracking robust nonlinear model predictive control. By combining the sampled-data model predictive control and sliding mode control, the influence of uncertainty is reduced efficiently, and the asymptotic stability of the closed loop system is improved, while the computational complexity remains unchanged. [19] proposed an integrated fault-tolerant control method with a two-layer structure to achieve longitudinal fault-tolerant control of hypersonic vehicles.

From the above analysis, it can be seen that the traditional nonlinear control methods have poor robustness and stability, and it is difficult to solve the problem of parameter uncertainty and system model mismatch. Observers [7, 20], neural networks [5, 21, 22], and other methods are used to actively compensate the system uncertainty, which have certain robustness. The sliding mode control method has obvious advantages in solving nonlinear problems with fast response and antidisturbance ability, but it still needs to solve the chattering problem. The model predictive control method has the characteristics of good system robustness and model mismatch. In this paper, the model predictive sliding mode control method is designed as the trajectory tracking method for hypersonic vehicle. Based on the model prediction algorithm, the sliding surface is introduced as the error model to improve the response speed. At the same time, to weaken the influence of system uncertainty and model mismatch, radial basis function neural network (RBFNN) is introduced to improve the robustness and stability of the system.

This paper is organized as follows: Section 2 briefly presents the longitudinal dynamic model of the hypersonic vehicle. In Section 3, a nonlinear predictive sliding mode control is designed for hypersonic vehicle, and its stability is analyzed. Numerical simulations are performed to verify the effectiveness of the method proposed in Section 4. Section 5 provides the conclusion.

2. The Longitudinal Dynamic Model of Hypersonic Vehicles

The longitudinal dynamic model of hypersonic vehicle considered here was developed at NASA Langley Center [23]. The nonlinear equations of motion are

$$\dot{V} = \frac{T\cos\alpha - D}{m} - \frac{\mu\sin\gamma}{r^2}, \tag{1}$$

$$\dot{\gamma} = \frac{L + T\sin\alpha}{mV} - \frac{\left(\mu - V^2 r\right)\cos\gamma}{Vr^2}, \tag{2}$$

$$\dot{h} = V\sin\gamma, \tag{3}$$

$$\dot{\alpha} = q - \dot{\gamma}, \tag{4}$$

$$\dot{q} = \frac{M}{I_{yy}}, \tag{5}$$

where V, γ, h, α, and q denote the velocity, flight path angle, altitude, angle of attack, and pitch rate; m, I_{yy}, μ, and r denote the mass, the moment of inertia of the vehicle, the gravitational constant, and the radial distance from the earth's center; and L, D, T, and M are the lift, the drag, the thrust force, and the pitching moment of the vehicle, which are modeled as

$$\begin{aligned} L &= \frac{1}{2}\rho V^2 S C_L, \\ D &= \frac{1}{2}\rho V^2 S C_D, \\ T &= \frac{1}{2}\rho V^2 S C_T, \\ M_{yy} &= \frac{1}{2}\rho V^2 S\bar{c} C_M, \\ r &= h + R_E, \end{aligned} \tag{6}$$

where ρ, S, $\bar{c}$, and R_E represent the air density, the reference of the vehicle, the aerodynamic chord, and the radius of the earth and C_L, C_D, C_T, and C_M denote the lift, drag, thrust, and moment coefficients. These coefficients are closely related to the flight status and flight environment.

The aerodynamic coefficients for cruise flight at nominal conditions ($V_0 = 4590.3$(m/s), $h_0 = 33528$ (m), $\gamma_0 = 0$, and $q_0 = 0$) are given by the following equations [24]:

$$\begin{aligned} C_L &= 0.6203\alpha, \\ C_D &= 0.6450\alpha^2 + 0.0043378\alpha + 0.003772, \\ C_T &= \begin{cases} 0.02576\beta, & \beta < 1, \\ 0.0224 + 0.0033\beta, & \beta >= 1, \end{cases} \\ C_M &= C_M(\alpha) + C_M(q) + C_M(\delta_e), \\ C_M(\alpha) &= -0.035\alpha^2 + 0.036617\alpha + 5.3261 \times 10^{-6}, \\ C_M(q) &= \left(\frac{\bar{c}q}{2V}\right)\left(-6.796\alpha^2 + 0.3105\alpha - 0.2289\right), \\ C_M(\delta_E) &= c_e(\delta_E - \alpha). \end{aligned} \tag{7}$$

Assuming the engine dynamics in second-order form, the dynamic equation is given by the following equation:

$$\ddot{\beta} = -2\xi\omega\dot{\beta} - \omega^2\beta + \omega^2\beta_T, \tag{8}$$

where ξ and ω_n represent the damping and the frequency of the system and β and β_T denote the setting value of the engine throttle valve and its command value.

3. Design and Stability Analysis of Predictive Sliding Mode Controller

3.1. Linearization of Nonlinear Systems. In this paper, the Lie derivative method is used to linearize the nonlinear model of hypersonic vehicle by linearizing its full-state feedback [23, 25]. After several derivations of the time of the output variables separately, the control variables appear in the differential equation:

$$\begin{cases} \dot{V} = f_1(x), \\ \ddot{V} = \dfrac{\omega_1 \cdot \dot{x}}{m}, \\ \dddot{V} = \dfrac{\omega_1 \cdot \ddot{x} + \dot{x}^T \cdot \Omega_2 \cdot \dot{x}}{m}, \end{cases}$$

$$\begin{cases} \dot{h} = f_2(x), \\ \ddot{h} = \dot{V} \sin\gamma + V\dot{\gamma}\cos\gamma, \\ \dddot{h} = \ddot{V}\sin\gamma + 2\dot{V}\dot{\gamma}\cos\gamma - V\dot{\gamma}^2\sin\gamma + V\ddot{\gamma}\cos\gamma, \\ h^{(4)} = \dddot{V}\sin\gamma + 3\ddot{V}\dot{\gamma}\cos\gamma - 3\dot{V}\dot{\gamma}^2\sin\gamma + 3\dot{V}\ddot{\gamma}\cos\gamma - 3V\dot{\gamma}\ddot{\gamma}\sin\gamma - V\dot{\gamma}^3\sin\gamma + V\ddot{\gamma}\cos\gamma, \end{cases} \tag{9}$$

where

$$\begin{aligned} \mathbf{x} &= [V\ \gamma\ \alpha\ \beta\ h]^T, \\ \dot{\gamma} &= f_3(\mathbf{x}), \\ \ddot{\gamma} &= \pi_1 \mathbf{x}, \\ \dddot{\gamma} &= \pi_1 \ddot{\mathbf{x}} + \dot{\mathbf{x}}^T \mathbf{\Pi}_2 \dot{\mathbf{x}}, \\ \boldsymbol{\omega}_1 &= m\frac{\partial f_1(\mathbf{x})}{\partial \mathbf{x}}, \\ \mathbf{\Omega}_2 &= \frac{\partial \boldsymbol{\omega}_1}{\partial \mathbf{x}}, \\ \boldsymbol{\pi}_1 &= \frac{\partial f_3(\mathbf{x})}{\partial \mathbf{x}}, \\ \mathbf{\Pi}_2 &= \frac{\partial \boldsymbol{\pi}_1}{\partial \mathbf{x}}. \end{aligned} \tag{10}$$

The vectors $\boldsymbol{\omega}_1$ and $\boldsymbol{\pi}_1$ and matrices $\mathbf{\Omega}_2$ and $\mathbf{\Pi}_2$ are given in [23]. The equations $f_1(x)$, $f_2(x)$, and $f_3(x)$ are represented in equations (1), (3), and (2), respectively.

Separate the second derivatives of the angle of attack α and throttle setting β into control-independent and control-dependent parts:

$$\begin{aligned} \ddot{\alpha} &= \ddot{\alpha}_0 + \left(\frac{c_e \cdot \rho \cdot V^2 \cdot S \cdot c}{2I_{yy}}\right) \cdot \delta_E, \\ \ddot{\beta} &= \ddot{\beta}_0 + \omega^2 \beta_T, \end{aligned} \tag{11}$$

where

$$\begin{aligned} \ddot{\beta}_0 &= -2\xi\omega\dot{\beta} - \omega^2\beta, \\ \ddot{\alpha}_0 &= \frac{1/2\rho V^2 Sc[C_M(\alpha) + C_M(q) - c_e\alpha]}{I_{yy} - \ddot{\gamma}}. \end{aligned} \tag{12}$$

$\ddot{\alpha}$ is the derivative of $\dot{\alpha}$. $\ddot{\alpha}_0$ is not related to δ_E. $\ddot{\alpha}_e = \partial\ddot{\alpha}/\partial\delta_E$ is the part related to δ_E.

Therefore, $\ddot{x}$ can be written as

$$\begin{aligned} \ddot{\mathbf{x}} &= \ddot{\mathbf{x}}_0 + [\delta_E \beta_T] \begin{bmatrix} 0 & 0 & \ddot{\alpha}_e & 0 & 0 \\ 0 & 0 & 0 & \omega^2 & 0 \end{bmatrix} \\ &= \left[\dddot{V}\ \ddot{\gamma}\ \ddot{\alpha}_0\ \ddot{\beta}_0\ \dddot{h}\right] + [\delta_E \beta_T] \begin{bmatrix} 0 & 0 & \ddot{\alpha}_e & 0 & 0 \\ 0 & 0 & 0 & \omega^2 & 0 \end{bmatrix}. \end{aligned} \tag{13}$$

Based on the above analysis, the linearized system dynamic equation can be expressed as

$$\begin{bmatrix} \dddot{V} \\ h^{(4)} \end{bmatrix} = \begin{bmatrix} \dddot{V}_0 \\ h_0^{(4)} \end{bmatrix} + \begin{bmatrix} B_{11} & B_{12} \\ B_{21} & B_{22} \end{bmatrix} \begin{bmatrix} \delta_E \\ \beta_T \end{bmatrix}, \tag{14}$$

where

$$\begin{aligned} \dddot{V}_0 &= \frac{\omega_1 \dot{x}_0 + \dot{x}^T \Omega_2 \dot{x}}{m}, \\ h_0^{(4)} &= \left(\frac{(\omega_1 \ddot{x}_0 + \dot{x}^T \Omega_2 \dot{x})\sin\gamma}{m}\right) + 3\ddot{V}\dot{\gamma}\cos\gamma - 3\dot{V}\dot{\gamma}^2\sin\gamma \\ &\quad + 3\dot{V}\ddot{\gamma}\cos\gamma - 3V\dot{\gamma}\ddot{\gamma}\sin\gamma - V\dot{\gamma}^3\cos\gamma \\ &\quad + V(\pi_1 \ddot{x}_0 + \dot{x}^T \Pi_2 \dot{x})\cos\gamma, \mathbf{B} \\ &= \begin{bmatrix} \dfrac{T_\alpha \cos\alpha - T\sin\alpha - D_\alpha}{m}\ddot{\alpha}_e, & \dfrac{T_\beta \omega^2 \cos\alpha}{m}, \\ \dfrac{[T\cos(\alpha+\gamma) + T_\alpha \sin(a+\gamma) + L_\alpha \cos\gamma - D_\alpha \sin\gamma]}{m}\ddot{\alpha}_e, & \dfrac{T_\beta \sin(\alpha+\gamma)}{m}, \end{bmatrix} \\ T_V &= \rho V S C_T, \\ T_\beta &= \frac{1}{2}\rho V^2 S C_\beta, \\ D_V &= \rho V S C_D, \\ L_V &= \rho V S C_L, \\ L_\alpha &= \frac{1}{2}\rho V^2 \frac{\partial C_L}{\partial \alpha}, \\ D_\alpha &= \frac{1}{2}\rho V^2 \frac{\partial C_D}{\partial \alpha}. \end{aligned} \tag{15}$$

The linearized system dynamic equation (14) can be expressed in the following form:

$$\mathbf{Y} = \mathbf{Y}_0 + \mathbf{B} \cdot \mathbf{u}. \tag{16}$$

3.2. Design of Predictive Sliding Mode Controller. Consider the following nonlinear systems:

$$\begin{aligned} \dot{\mathbf{x}} &= \mathbf{f}(x) + \mathbf{g}(x)\mathbf{u}, \\ \mathrm{y} &= \mathbf{h}(x), \end{aligned} \tag{17}$$

where $\mathbf{x} \in \mathbf{R}^n$ denotes the system state; $\mathbf{u} \in \mathbf{R}^m$ denotes the input control variables; $f \in \mathbf{R}^n$, $g \in \mathbf{R}^{n\times m}$, and $h \in \mathbf{R}^m$ are smooth bounded functions; n and m are the number of state variables and control inputs, and $\mathbf{y} = [V\ h]^T$.

The output in the moving time frame is predicted by the Taylor series expansion. Repeating the differentiation up to ρ times of the output concerning time, together with repeated substitution of the system (17), yields

$$\begin{aligned} \dot{y}(t) &= L_f h(x), \\ &\vdots \\ y^{[\rho-1]}(t) &= L_f^{\rho-1} h(x), \\ y^{[\rho]}(t) &= L_f^{\rho} h(x) + L_g L_f^{\rho-1} h(x) u(t), \end{aligned} \tag{18}$$

where $L_f^{\rho_i} h_i(x) \in \mathbf{R}$ indicates that $h_i(x)$ calculates the ρ_i order Lie derivative along the vector field f.

When the control order is r, the output Taylor expansion series must be at least $\rho + r$, so that the control signal can appear in the prediction, and then, there exists a current time difference:

$$\begin{aligned} y^{[\rho+1]}(t) &= L_f^{\rho+1} h(x) + p(u(t), x(t)) + L_g L_f^{\rho-1} h(x) \dot{u}(t), \\ p_{11}(u(t), x(t)) &= L_g L_f^{\rho} h(x) u(t) + \frac{d L_g L_f^{\rho-1} h(x)}{dt} u(t), \end{aligned} \tag{19}$$

where p_{11} is nonlinear for both $u(t)$ and $x(t)$.

Similarly, the higher-order derivatives that can be output everywhere can be summarized as

$$\hat{\mathbf{Y}}(t) = \begin{bmatrix} \hat{y}^{[0]} \\ \hat{y}^{[1]} \\ \vdots \\ \hat{y}^{[\rho]} \\ \vdots \\ \hat{y}^{[\rho+r]} \end{bmatrix} = \begin{bmatrix} h(x) \\ L_f^1 h(x) \\ \vdots \\ L_f^{\rho} h(x) \\ \vdots \\ L_f^{\rho+r} h(x) \end{bmatrix} + \begin{bmatrix} 0_{m\times 1} \\ \vdots \\ 0_{m\times 1} \\ H(\hat{u}) \end{bmatrix}, \tag{20}$$

where $\mathbf{H}(\hat{u}) \in R^{m(r+1)}$ is a matrix about $\hat{u}(t), \dot{\hat{u}}(t), \cdots, \hat{u}^{[r]}(t)$.

$$\mathbf{H}(\hat{u}) = \begin{bmatrix} L_g L_f^{\rho-1} h(x) \hat{u}(t) \\ p_{11}(\hat{u}(t), x(t)) + L_g L_f^{\rho-1} h(x) \dot{\hat{u}}(t) \\ \vdots \\ p_{r1}(\hat{u}(t), x(t)) + p_{rr}\left(\hat{u}(t), \cdots, \hat{u}^{[r-1]}(t), x(t)\right) + \cdots + L_g L_f^{\rho-1} h(x) \hat{u}^{[r]}(t) \end{bmatrix}, \tag{21}$$

where $\hat{\bar{\mathbf{u}}} = [\hat{u}(t)\ \dot{\hat{u}}(t) \cdots \hat{u}^{[r]}(t)]$.

In this paper, the step function is chosen as the actual control for predictive control:

$$\begin{aligned} u(t+\tau) &= u(t), \\ \dot{u}(t) &= \cdots = u^{[r]}(t) = 0. \end{aligned} \tag{22}$$

Time-dependent derivative of current system output:

$$\begin{aligned} \dot{y}_1 &= L_f h_1(x) = \dot{V}, \\ \ddot{y}_1 &= L_f^2 h_1(x) = \ddot{V}, \\ \dddot{y}_1 &= L_f^3 h_1(x) + L_{g1} L_f^2 h_1(x) u_1 + L_{g2} L_f^2 h_1(x) u_2 = \dddot{V}, \\ \dot{y}_2 &= L_f h_2(x) = \dot{h}, \\ \ddot{y}_2 &= L_f^2 h_2(x) = \ddot{h}, \\ \dddot{y}_2 &= L_f^3 h_2(x) = \dddot{h}, \\ y_2^{(4)} &= L_f^4 h_2(x) + L_{g1} L_f^3 h_2(x) u_1 + L_{g2} L_f^3 h_2(x) u_2 = h^{(4)}. \end{aligned} \tag{23}$$

According to the linearization in the previous section, the relative orders of the two outputs of the hypersonic vehicle longitudinal model are $\rho_1 = 3$ and $\rho_2 = 4$. During the rolling prediction time, the future output of the system is expanded by the Taylor series, omitting the high-level term, to obtain the predicted value:

$$\begin{aligned} y_V(t+\tau) &\cong y_V(t) + \tau \dot{y}_V(t) + \cdots + \frac{\tau^3}{3!} y_V^3(t), \\ y_h(t+\tau) &\cong y_h(t) + \tau \dot{y}_h(t) + \cdots + \frac{\tau^4}{4!} y_h^4(t). \end{aligned} \tag{24}$$

At the prediction time τ, the output of the nonlinear system equation can be expressed as

$$y(t+\tau) = \begin{bmatrix} y_1(t+\tau) \\ y_2(t+\tau) \end{bmatrix} = \mathbf{\Gamma}(\tau) Y(t), \tag{25}$$

where

$$\begin{aligned} \mathbf{\Gamma}(\tau) &= \text{diag}\,[\mathbf{\Gamma}_1 \mathbf{\Gamma}_2], \\ \mathbf{\Gamma}_i(\tau) &= \left[1\ \tau \cdots \frac{\tau^{\rho_i}}{\rho_i!}\right], \quad 1 \le i \le 2, \\ \mathbf{Y}(t) &= \text{diag}\,[Y_1 Y_2], \\ \mathbf{Y}_i &= \begin{bmatrix} y_i(t) \\ \vdots \\ y_i^{[\rho_i]}(t) \end{bmatrix}, \quad 1 \le i \le 2. \end{aligned} \tag{26}$$

For the same reason,

$$\mathbf{y}_c(t+\tau) = \begin{bmatrix} y_{c1}(t+\tau) \\ y_{c2}(t+\tau) \end{bmatrix} = \mathbf{\Gamma}(\tau)\mathbf{Y}_c(t). \quad (27)$$

In practical application system, due to perturbation and model adaptation, there is a certain error between the predicted output of the model and the actual output. The error at the time $t+\tau$ is

$$\mathbf{e}(t+\tau) = y_c(t+\tau) - y(t+\tau) = \mathbf{\Gamma}(\tau)(\mathbf{Y}_c(t) - \mathbf{Y}(t)). \quad (28)$$

In real systems, the initial point is often unknown at any time. To make the system more stable, the sliding mode surface is designed according to the error between the predicted output and the expected output, so that the system motion keeps moving close to the stability of the sliding mode surface. Referring to [14, 26, 27], the sliding surfaces are designed as equations (29) and (30). The speed sliding mode surface and the height sliding mode surface are designed, respectively,

$$\mathbf{s}_V(t+\tau) = C_V \cdot E_V(t+\tau) = c_{Vi} \cdot e_V^{[i]}(t+\tau), \quad (29)$$

$$\mathbf{s}_h(t+\tau) = C_h \cdot E_h(t+\tau) = c_{hj} \cdot e_h^{[j]}(t+\tau), \quad (30)$$

where $e_V^{[i]}(t+\tau) = V^{[i]} - V_c^{[i]}$, $e_h^{[j]}(t+\tau) = h^{[j]} - h_c^{[j]}$, $c_{Vi} \subset C_V \in R_{3\times 1}$, $c_{hj} \subset C_h \in R_{4\times 1}$, $i = 0, 1, 2$, and $j = 0, 1, 2, 3$.

Then, the performance index of the predictive sliding mode controller can be designed as

$$\mathbf{J} = \frac{1}{2}\int_0^{T_p} S(t+\tau)^T S(t+\tau) d\tau. \quad (31)$$

The necessary condition to achieve the best performance indicator is

$$\frac{\partial \mathbf{J}}{\partial \mathbf{u}} = 0. \quad (32)$$

Theorem 1. *Consider continuous-time nonlinear systems, and assume that the output of the prediction interval is predicted through ρ order Taylor expansion. For a given control order $r \geq 0$, the control law of the minimum index of the optimal nonlinear control system is [15]*

$$\mathbf{u}(t) = -\left(L_g L_f^{\rho-1} h(x)\right)^{-1}\left(KM_\rho + L_f^\rho h(x) - \omega^{[\rho]}(t)\right), \quad (33)$$

where $\mathbf{M}_\rho \in \mathbf{R}^{m\times\rho}$.

$$\mathbf{M}_\rho = \begin{bmatrix} h(x) - \omega(t) \\ L_f^1 h(x) - \omega^{[1]}(t) \\ \vdots \\ L_g^{\rho-1} h(x) - \omega^{[\rho-1]}(t) \end{bmatrix}. \quad (34)$$

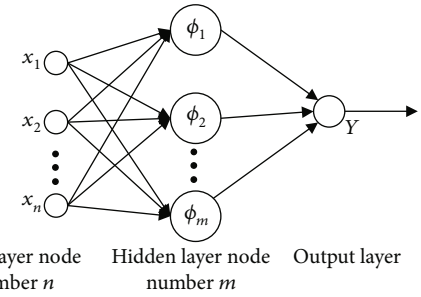

Figure 1: RBFNN structure.

$\mathbf{K} \in \mathbf{R}^{m\times\rho}$ represents the matrix of $\overline{\mathbf{\Gamma}}_i(T_p) = \mathbf{\Gamma}_i^{-1}\mathbf{\Gamma}_i$:

$$\overline{\mathbf{\Gamma}}_{(i,j)} = \frac{T_p^{i+j-1}}{(i-1)!(j-1)!(i+j-1)}, \quad i, j = 1, \cdots, \rho + r + 1. \quad (35)$$

Derivation process:

The performance index for the predictive sliding mode controller is

$$\mathbf{J} = \frac{1}{2}\int_0^{T_p} \mathbf{S}(t+\tau)^T \mathbf{S}(t+\tau) d\tau = \frac{1}{2}\int_0^{T_p} (\mathbf{C}E(t+\tau))^T (\mathbf{C}E(t+\tau)) d\tau, \quad (36)$$

where

$$C \cdot E(t+\tau) = C \cdot \left(M + \begin{bmatrix} 0_{m\rho\times 1} \\ H(u) \end{bmatrix}\right), \quad (37)$$

where

$$\mathbf{M} = \begin{bmatrix} L_f^0 h(x) \\ L_f^1 h(x) \\ \vdots \\ L_f^{\rho+r} h(x) \end{bmatrix} - \begin{bmatrix} \omega(t) \\ \dot{\omega}(t) \\ \vdots \\ \omega^{[\rho+r]}(t) \end{bmatrix}. \quad (38)$$

Derivation of equation (21) is

$$\frac{\partial \mathbf{H}}{\partial \bar{\mathbf{u}}} = \begin{bmatrix} L_g L_f^{\rho-1} h(x) & 0_{m\times m} & \cdots & 0_{m\times m} \\ x_{m\times m} & L_g L_f^{\rho-1} h(x) & \cdots & 0_{m\times m} \\ \vdots & \vdots & \ddots & \vdots \\ x_{m\times m} & x_{m\times m} & \cdots & L_g L_f^{\rho-1} h(x) \end{bmatrix}, \quad (39)$$

where $\mathbf{x}_{m\times m}$ represents a nonzero $m \times m$ size date block in $\partial\mathbf{H}/\partial\mathbf{u}$ and $\bar{\mathbf{u}} = [u(t)\ \dot{u}(t) \cdots u^{[r]}(t)]$.

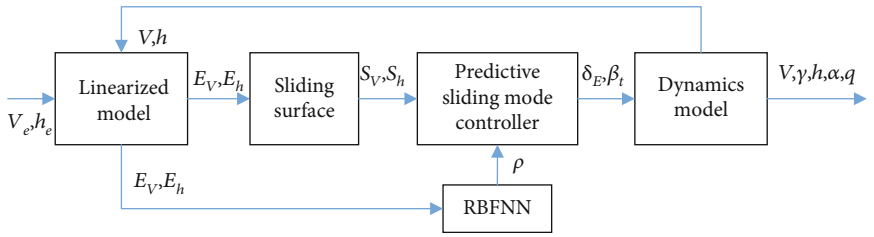

Figure 2: Trajectory tracking control system based on the predictive sliding mode controller.

Table 1: Some default parameters used in this paper.

Parameter	Value	Parameter	Value	Parameter	Value
m (kg)	136820	I_{yy} (kg·m^2)	9490740	ρ_0 (kg/m^3)	1.2266
S (m^2)	334.73	C_e	0.292	H_0 (m)	7315.2
C (m)	24.38	ξ	0.7	δ_E	[-20, 20]
ε	3.9802E14	ω	20	C_V	[80, 105, 50]
β_T	[0 ~ 1.2]	step (s)	0.05	C_h	[40, 50.625, 45, 10]
R_E (m)	6373100	stepNum	30		

Equation (39) can be written as

$$\left(\frac{\partial \mathbf{H}}{\partial \bar{\mathbf{u}}}\right)^T \left[\bar{T}_{\rho r}^T \bar{T}_{rr}\right]\mathbf{M} + \left(\frac{\partial \mathbf{H}}{\partial \bar{\mathbf{u}}}\right)^T \bar{T}_{rr}\mathbf{H}(\bar{\mathbf{u}}) = 0. \quad (40)$$

According to the definition of relativity, $L_g L_f^{\rho-1}h(x)$ is reversible, and the $(\partial \mathbf{H}/\partial \mathbf{u})^T$ is also reversible. At the same time, $\overline{\boldsymbol{\Gamma}}_{rr}$ is a positive definite matrix. The above equation can be written in

$$\mathbf{H}\left(\widehat{\bar{u}}\right) = -\left[\Gamma_{rr}^{-1}\boldsymbol{\Gamma}_{\rho r}^T I_{m(r+1)\times m(r+1)}\right]\mathbf{M}. \quad (41)$$

Considering equations (21) and (22), the above equation can be written as

$$L_g L_f^{\rho-1}h(x)u(t) + K\mathbf{M}_\rho + L_f^\rho h(x) - \omega(t)^{[\rho]} = 0, \quad (42)$$

where K represents the first m columns of $\Gamma_{rr}^{-1}\boldsymbol{\Gamma}_{\rho r}^T$, and similarly, M_ρ can be represented as

$$\mathbf{M}_\rho = \left[c_1(h(x) - w(t))^T c_2\left(L_f^1 h(x) - w^{[1]}(t)\right)^T \cdots c_\rho\left(L_f^{\rho-1}h(x) - w^{[\rho-1]}(t)\right)^T\right]^T. \quad (43)$$

Equation (33) can be solved by the above equation, where$[c_1,\cdots,c_\rho]^T \subset \mathbf{C} = [C_V\,; C_h]$.

For the current system, equation (33) can be rewritten as follows: the predictive sliding mode controller designed for the system dynamic equation (16):

$$\mathbf{u}(t) = -\mathbf{B}^{-1}(\mathbf{KS} + \mathbf{F}_x - \mathbf{Y}_c), \quad (44)$$

where $\mathbf{Y}_c = y_c^{[\rho]} = [y_V^{[\rho_1]}(t)\, y_H^{[\rho_2]}(t)]^T$ and $\mathbf{F}_x = [\ddot{V}_0\, h_0^{(4)}]^T$.

By reference [15, 28], this paper designs the formula feedback matrix as follows:

$$\mathbf{K} = \begin{bmatrix} K_1 & 0 \\ 0 & K_2 \end{bmatrix},$$
$$\mathbf{K}_1 = \left[\frac{27}{2T_p^3}\ \frac{42}{5T_p^2}\ \frac{7}{2T_p}\right], \quad (45)$$
$$\mathbf{K}_2 = \left[\frac{216}{5T_p^4}\ \frac{36}{T_p^3}\ \frac{108}{7T_p^2}\ \frac{9}{2T_p}\right],$$

where $T_p = \text{step}^*\text{stepNum}$, in which T_p represents predict time, step means the simulation step, and stepNum is number of predictive steps.

3.3. Radial Basis Function Neural Network Controller. Radial basis function (RBF) has the advantages of being able to approximate any nonlinear function, dealing with the laws that are difficult to analyze in the system, strong generalization ability, and fast learning convergence [29, 30].

As shown in Figure 1, the RBFNN structure is mainly composed of an input layer, a hidden layer, and an output

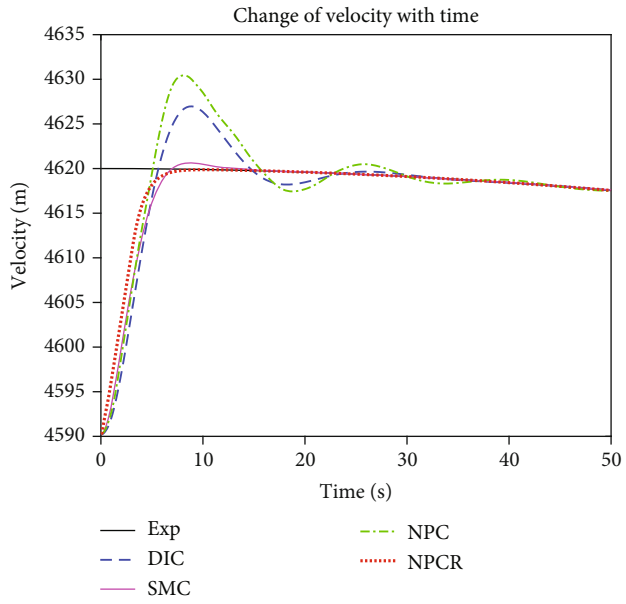

Figure 3: Velocity changes with time under different controllers.

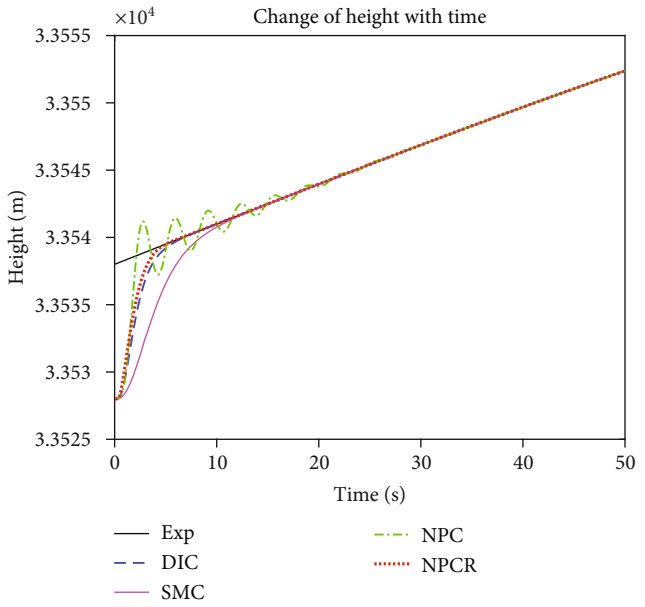

Figure 4: Height changes with time under different controllers.

layer. Use the Gaussian function as the transfer function of RBF [31]:

$$\phi_i(x) = \exp\left(-\frac{\|x - c_i\|^2}{2\sigma_i^2}\right), \quad i = 1, 2, \cdots, m. \tag{46}$$

When the Gaussian function is selected as the hidden layer transfer function of RBF, the hidden layer is used to realize the nonlinear mapping of $X \longrightarrow \phi_i(x)$, using the output layer to realize linear mapping of $\phi_i(x) \longrightarrow y_k$. Assume that the input of the input layer is $X = (x_1, x_2, \cdots, x_j, \cdots, x_n)$ and the actual output is $Y = (y_1, y_2, \cdots, y_k, \cdots, y_p)$; the output of the k neural network in the output layer can be expressed as

$$\hat{y}_k = \sum_{i=1}^{m} w_k \phi_i(X), \quad k = 1, 2, \cdots, m, \tag{47}$$

where m is the number of output layer nodes and hidden layer nodes, p is the number of output layer nodes, w_{ik} is the connection weight between the ith unit of the node in the hidden layer and the k neurons in the output layer, and $R_i(x)$ is the transfer function of the ith neuron in the hidden layer. Therefore, when the cluster center c_i and weight w_k of RBF are determined, the corresponding output value of RBF can be obtained under the condition of a given output.

3.4. Design of Predictive Sliding Mode Controller considering Uncertainty Compensation. Considering the mathematical model uncertainty and the existence of external disturbances $d_t \in R_{m\times 1}$ in the system,

$$\mathbf{Y} = \mathbf{Y}_0 + \mathbf{B} \cdot \mathbf{u} + \mathbf{d}_t. \tag{48}$$

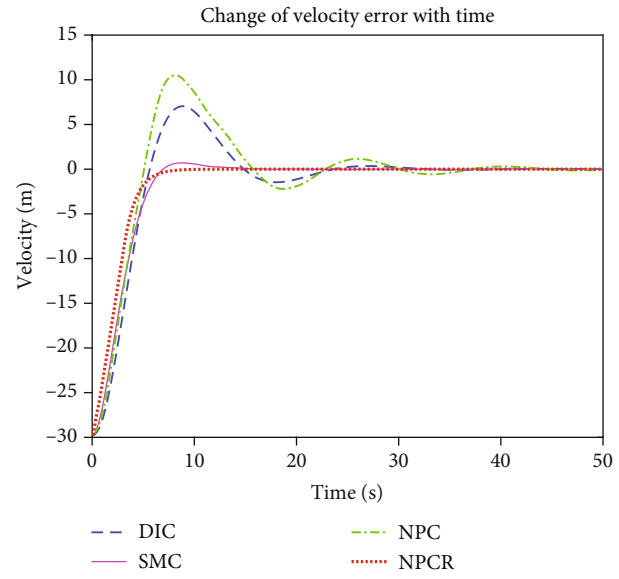

Figure 5: Velocity error changes with time under different controllers.

The RBFNN approximation error is introduced. The learning algorithm of neural network weight matrix is

$$\begin{aligned} \dot{W}_V &= -\alpha_V \phi_V S_V, \\ \dot{W}_h &= -\alpha_h \phi_h S_h. \end{aligned} \tag{49}$$

Then, the predictive sliding mode controller using RBF neural network to compensate for the disturbance error is

$$\mathbf{u}(t) = -\mathbf{B}^{-1}(\mathbf{KS} + \mathbf{F}_x - \mathbf{Y}_c + \boldsymbol{\rho}), \tag{50}$$

where ρ denotes the compensation for system uncertainty factors:

$$\boldsymbol{\rho} = \left[W_V \phi_V W_h \phi_h\right]^T = \left[W_V^* \phi_V W_h^* \phi_h\right]^T + \left[\varepsilon_V \varepsilon_h\right]^T, \quad (51)$$

where W^* is ideal optimal weight matrix and ε_V and ε_h represent approximation errors. Assume that ε_V and ε_h are bounded, and the neural network can approximate the uncertainty of the model with any precision.

$$\begin{aligned} \|\varepsilon_V\| \le \varepsilon_{Vp}, \int_0^\infty \|\varepsilon_V\|^2 dt < \infty, \\ \|\varepsilon_h\| \le \varepsilon_{hp}, \int_0^\infty \|\varepsilon_h\|^2 dt < \infty, \end{aligned} \quad (52)$$

where ε_{Vp} and ε_{hp} are normal numbers.

Based on the SMC and RBFNN, this paper designs an improved nonlinear predictive sliding mode controller. The proposed control scheme is summarized in Figure 2.

3.5. Stability Analysis of the Control System. This section analyzes the stability of the control law (50) proposed in this paper and first makes the following assumptions [32]:

The internal zero dynamics of the nonlinear system driven by desired state (w) are defined for all $t \ge 0$, bounded and uniformly asymptotically stable.

Assume matrix K in equation (50) be expressed as $\mathbf{K} = [k_0\, k_1 \cdots k_{\rho-1}]$, where $k_i \in R^{m\times m}$. Formula (50) is substituted into formula (18):

$$\begin{aligned} y^{[\rho]}(t) = L_f^\rho h(x) - \sum_{i=0}^{\rho-1} k_i c_i \left(L_f^i h(x) - w^{[i]}(t)\right) \\ - L_f^\rho h(x) + w^{[\rho]}(t) + W\phi, \end{aligned} \quad (53)$$

where c_i represents the values of sliding surfaces (29) and (30), respectively, $[c_1,\cdots,c_\rho]^T \subset \mathbf{C} = [C_V\,; C_h]$; $W\phi$ represents compensation for uncertainty.

Consider tracking error:

$$e(t) = w(t) - y(t). \quad (54)$$

Substitute (54) into (53):

$$e^{[\rho]}(t) + k_{\rho-1} c_{\rho-1} e^{[\rho-1]}(t) + \cdots + k_0 c_0 e(t) = 0. \quad (55)$$

It can be proved that the current controller is stable. Reference [15] shows the detailed proof process.

To prove that the RBFNN controller is convergent, the Lyapunov function is designed as [13]

$$\mathbf{L} = \frac{1}{2}\mathbf{s}_V^T \cdot \mathbf{s}_V + \frac{1}{2\alpha} Tr\left(\tilde{\mathbf{W}}^T \cdot \tilde{\mathbf{W}}\right), \quad (56)$$

where $\tilde{\mathbf{W}}_V = \mathbf{W}_V{}^* - \mathbf{W}_V$. Because of the similarity of the proving process between the stability of velocity channel and altitude channel, only the velocity channel is analyzed here.

Differential equation (56):

$$\dot{\mathbf{L}} = \mathbf{s}_V^T \cdot \dot{\mathbf{s}}_V + \frac{1}{\alpha_V} Tr\left(\tilde{\mathbf{W}}_V^T \cdot \dot{\tilde{\mathbf{W}}}_V\right). \quad (57)$$

Solve the two distributions above:

$$\begin{aligned} \frac{1}{\alpha_V} Tr\left(\tilde{\mathbf{W}}_V^T \cdot \dot{\tilde{\mathbf{W}}}_V\right) &= \frac{1}{\alpha_V} Tr\left[\tilde{\mathbf{W}}_V^T \cdot \left(\mathbf{W}_V{}^* - \mathbf{W}_V\right)\right] \\ &= -\frac{1}{\alpha_V} Tr\left[\tilde{\mathbf{W}}_V^T \cdot \left(-\alpha_V \phi_V s_V^T\right)\right]. \end{aligned} \quad (58)$$

According to formulas (29) and (48)–(50),

$$\dot{\mathbf{s}}_V = c_{V1}\dot{e}_V + c_{V2}\ddot{e}_V + c_{V3}\dddot{e}_V + \mathbf{W}_V^T \phi_V - \rho_V. \quad (59)$$

General assumptions [26]:

$$|D_V(x,u,t)| \le |D_{V0}(x,u,t)|, \quad (60)$$

where $D_{V0}(x,u,t)$ are nonnegative numbers. Take control quantity u as solution

$$-K_V|\mathbf{s}_V| = \mathbf{s}_V(c_{V1}\dot{e}_V + c_{V2}\ddot{e}_V + c_{V3}\dddot{e}_V), \quad (61)$$

where K_V is optional positive integer; then,

$$f_s = -K_V|\mathbf{s}_V| + D_V\mathbf{s}_V \le (|D_V| - K_V)|\mathbf{S}_V|. \quad (62)$$

Substitute (62) and (59) into (54):

$$\begin{aligned} \mathbf{s}_V^T \cdot \dot{\mathbf{s}}_V &= f_s + \mathbf{W}_V^T \phi_V - \rho_V, \\ \dot{\mathbf{L}} &= f_s + \mathbf{s}_V^T\left(\tilde{\mathbf{W}}_V^T \phi_V - \mathbf{W}_V^* \phi_V - \varepsilon_V\right) \\ &\quad - \frac{1}{\alpha_V} Tr\left[\tilde{\mathbf{W}}_V^T \cdot \left(-\alpha_V \phi_V \mathbf{s}_V^T\right)\right] \\ &= f_s - \mathbf{s}_V^T \boldsymbol{\varepsilon}_V \le (|D_V| - K_V)|\mathbf{s}_V| - \mathbf{s}_V^T \boldsymbol{\varepsilon}_V. \end{aligned} \quad (63)$$

When $K_V > |D_{V0}|$ and $\mathbf{s}_V \ne 0$, $\dot{\mathbf{L}}$ is negative definite, while outside region $\sum \mathbf{s}_V = \{\mathbf{s}_V(t) | 0 \le \|\mathbf{s}_V(t)\| \le (\boldsymbol{\varepsilon}_V/(|D_V| - K_V))\}$. According to the assumption and Lyapunov theory, $\lim_{t\longrightarrow\infty} \mathbf{s}_V(t) = 0$. According to formula (29), $\lim_{t\longrightarrow\infty} e_V(t) = 0$, which means the closed loop system of velocity channel is asymptotically stable. Similarly, it can be deduced that the closed loop system of high channel is asymptotically stable as $\lim_{t\longrightarrow\infty} \mathbf{s}_h(t) = 0$ and $\lim_{t\longrightarrow\infty} e_h(t) = 0$ show.

4. Simulation

For the longitudinal dynamic model and predictive sliding mode control of the hypersonic vehicle in this paper, this section verifies the correctness and effectiveness of the controller through simulation. In this section, we select level flight cruising stage ($V_0 = 4590.3$ m/s, $h_0 = 33528$ m, $\gamma_0 = 0$,

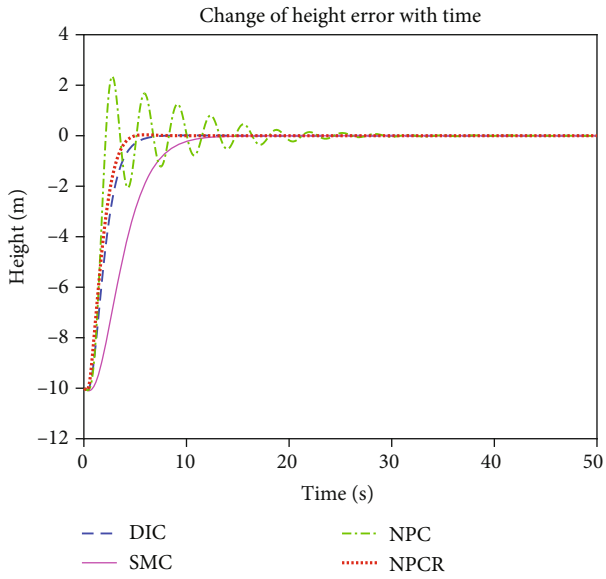

Figure 6: Height error changes with time under different controllers.

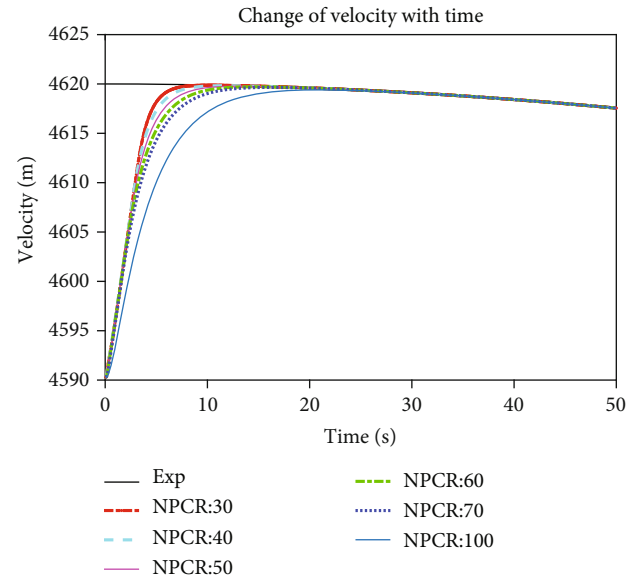

Figure 7: Velocity changes with time under different prediction steps.

Table 2: Standard deviation comparison of different controllers.

No.	DIC	SMC	NPC	NPCR
1	0.1234761	0.387294	0.0648344	0.238022
2	0.132577	0.3969378	0.0645986	0.2374112
3	0.1224386	0.3837611	0.0649847	0.2368241
4	0.129998	0.3970867	0.064596	0.2380209
5	0.1229457	0.3866949	0.0642442	0.2455137
6	0.120701	0.3871694	0.0634814	0.256432
7	0.1216268	0.3908661	0.0649917	0.253489
8	0.1189904	0.3919185	0.0642716	0.2385589
9	0.1200567	0.3810074	0.0623854	0.2328096
10	0.1232244	0.3859532	0.0633241	0.2370749
Average	0.12360347	0.38886891	0.06417121	0.24141563

$q_0 = 0$, and $\alpha = 1.8736^\circ$), the initial elevator angle $\delta_E = -0.4129^\circ$, and the engine throttle command valve $\beta_T = 0.1788$. Given the expected trajectory,

$$Y_d = \begin{bmatrix} V_d \\ h_d \end{bmatrix} = \begin{bmatrix} 4600 + 20 \cdot \cos(0.01 \times t) \\ 33538 + 30 \cdot \sin(0.01 \times t) \end{bmatrix}. \quad (64)$$

Relevant vehicle and controller parameters adopted are shown in Table 1.

In this simulation, the computing platform is Intel i7-12700 @2.1 GHz, 32 GB RAM, and the operating system is Windows 10.

4.1. Comparison between Different Controllers. To verify the rationality of the nonlinear predictive sliding mode controller with RBFNN (NPCR) designed in this paper, the dynamic inversion controller (DIC) in [33], the adaptive sliding mode controller (SMC) in [34], and the nonlinear predictive controller (NPC) in [28] are introduced for comparison.

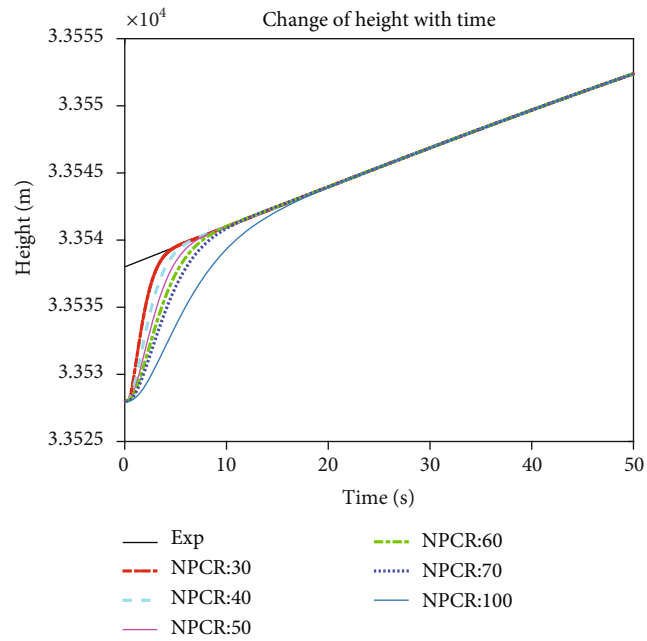

Figure 8: Height changes with time under different prediction steps.

The state tracking curves are shown in Figures 3 and 4, and the error curves are shown in Figures 5 and 6. It is obviously that the NPCR controller is the fastest one to reach the expected convergence state both in velocity and height control. The SMC controller is the second one to reach convergence in velocity control, while the DIC controller is the second in height control. The traditional NPC is the slowest with oscillation. In terms of stability, the NPCR and SMC controller have no oscillation, and DIC controller is better

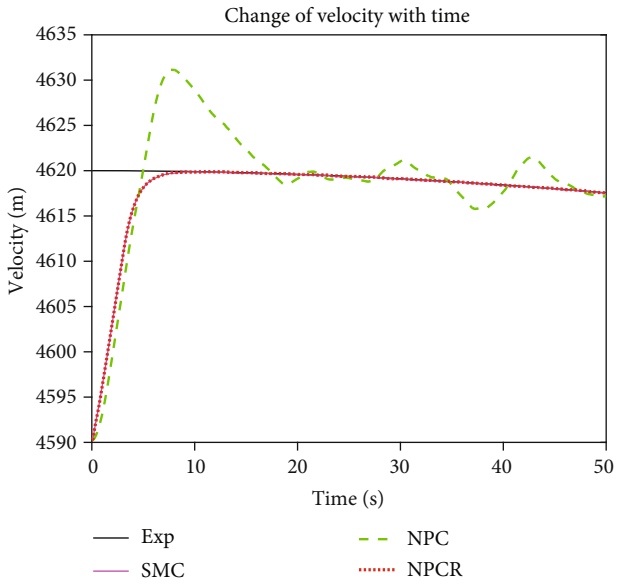

Figure 9: Velocity changes with time under different controllers.

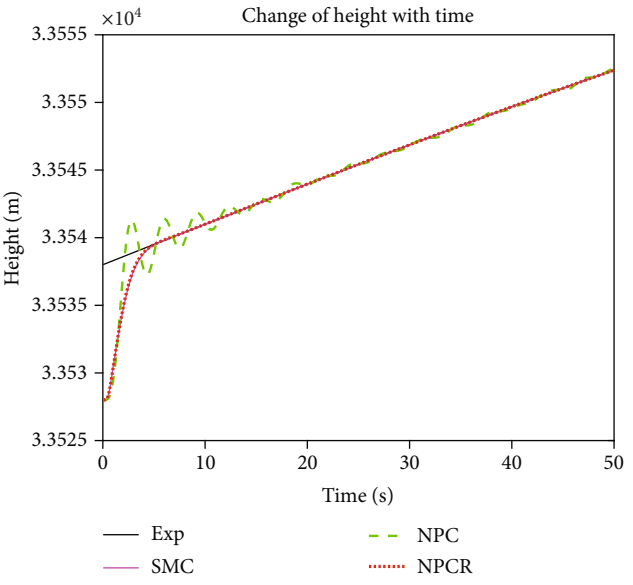

Figure 11: Height changes with time under different controllers.

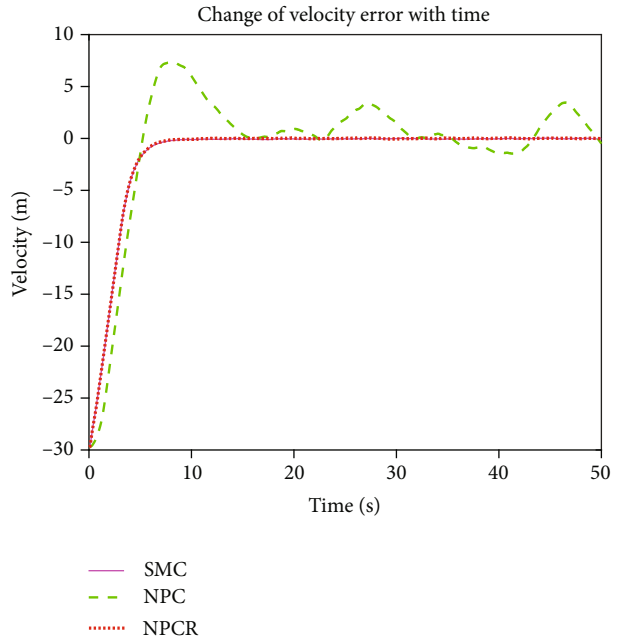

Figure 10: Velocity error changes with time under different controllers.

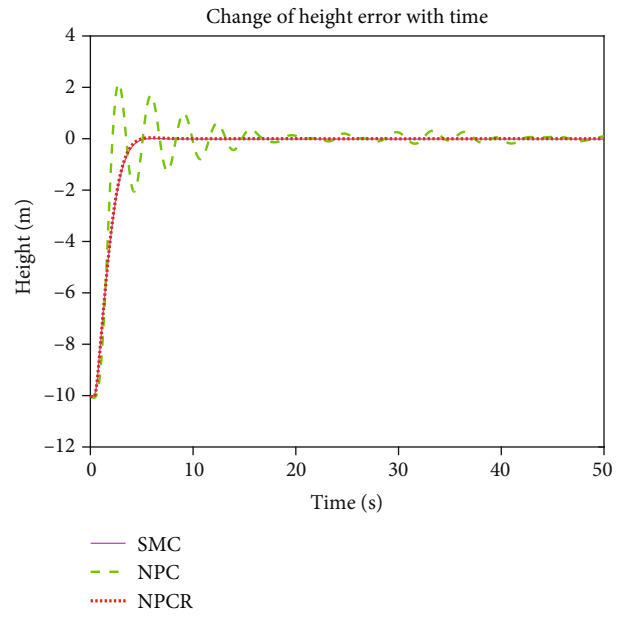

Figure 12: Height error changes with time under different controllers.

than NPC controller. The error curves can support these views.

In addition, the running time of different controllers is simulated and analyzed. Run all the simulations for 10 times. The running time is shown in Table 2. It is found that among all the four controllers, NPC controller has the fastest computing speed while its effect is the worst. SMC controller is the slowest while its effect is only second to NPCR controller. Due to the introduction of RBFNN, the running time of NPCR controller proposed in this paper has increased compared with NPC controller, but it still has high computational efficiency. The calculation time of all controllers is far less than the flight time of hypersonic vehicles, which can meet the mission requirements.

It is found that the convergence stability of NPCR is better than the other controllers. Moreover, compared with other controllers, the NPCR proposed in this paper has the following advantages: nonoscillatory, fast convergence speed, and stable flight.

4.2. Comparison of Predictive Steps. To better analyze the control performance of NPCR, this paper designs different prediction steps [30, 40, 50, 60, 70, and 100] to compare,

Table 3: Standard deviation comparison of different controllers.

No.	stdVel_SMC	stdVel_NPC	stdVel_NPCR	stdHei_SMC	stdHei_NPC	stdHei_NPCR
1	0.05243234	2.20237406	0.040025396	0.011370051	0.119032746	0.001720650
2	0.06040536	1.34278061	0.024144282	0.011743559	0.192104650	0.002195439
3	0.02832648	0.77988914	0.010792443	0.011309792	0.177574130	0.001863315
4	0.04555576	1.56965732	0.037606093	0.013559919	0.166577457	0.001183292
5	0.03811331	1.82886662	0.022685027	0.012647894	0.178744813	0.001534456
6	0.02646883	2.06267558	0.021519558	0.010611807	0.203627088	0.001062011
7	0.02081986	2.42904414	0.011553179	0.012366545	0.071514863	0.001199864
8	0.03791702	2.22209763	0.016365690	0.011411081	0.169800069	0.002157447
10	0.06009723	2.00051687	0.036688356	0.015281236	0.116195437	0.000701935
Average	0.037013619	1.64379020	0.0221380024	0.011030188	0.139517125	0.0013618409

and the results are shown in Figures 7 and 8. Simulation shows that when the predictive step size is small (<29), the prediction time is too short to realize trajectory tracking control. By comparing the velocity change curve and the height change curve, it is found that the convergence time of NPCR controller increases with the increase of the prediction step; that is, the smaller the prediction step, the faster the convergence speed. Therefore, 30 (the prediction time is 1.5 s) is selected in this paper as the prediction step.

4.3. Comparison of Jitter Suppression. To solve the uncertainties existing in the system, RBFNN is introduced in this paper to predict and compensate for the disturbances in the control process. In this section, the SMC controller means the nonlinear predictive controller with sliding surface. As is shown in Figures 9 and 10, the SMC and NPCR controller have converged to the expected state in a very short time on velocity control, while the NPC controller is still oscillating. The same goes for height control as shown in Figures 11 and 12. It is found that the traditional NPC controller has a weak ability to suppress uncertainties, while the NPC effect is better than the traditional NPC controller after the introduction of sliding mode and RBF. The introduction of RBF and the sliding mode can achieve good control performance. At the same time, it has strong robustness to model uncertainty and external disturbances.

Although the introduction of RBFNN has considerable advantages, it is difficult to distinguish the differences between SMC and NPCR controller. To further analyze the effect of introducing RBFNN, run for 10 times, intercept the error value of the 25th~30th seconds, and count its standard deviation. The details are shown in Table 3. The average standard deviation of NPCR controller is less than SMC controller both in velocity and height, while that of the above two controllers is obviously less than NPC controller. It is found that the introduction of RBF improves the convergence speed, the stability of the controller, and the performance of the controller.

5. Conclusion

The hypersonic vehicle has the characteristics of a large flight airspace span, fast speed, being sensitive to environmental parameters, fast time variation, coupling, nonlinearity, uncertainty, and so on, which means that the performance of the flight controller needs higher requirements. Traditional linear control methods and nonlinear predictive control methods have shortcomings. Therefore, this paper adopts a nonlinear predictive control method, introduces sliding mode surface as an error function, and uses RBFNN to compensate for uncertainty and external disturbance. Simulation results show that the predictive sliding mode control method proposed in this paper can not only significantly improve the convergence performance, convergence speed, and stability of nonlinear predictive control but also significantly improve robustness to parameter uncertainties and external disturbances.

Data Availability

The data was already included in the manuscript.

Conflicts of Interest

The authors declare that they have no conflicts of interest.

Acknowledgments

This research was funded by the Basic Research Project of the Science and Technology on Complex Electronic System Simulation Laboratory (no. DXZT-JC-ZZ-2020-012), the National Natural Science Foundation of China (no. 11772185), the Project (nos. 020214 and D030307), and the Fundamental Research Foundation of the Central Universities (nos. 3072022TS0401, 3072022CFJ0202, and 3072022CFJ0204).

References

[1] C. Tao, J. Wan, and J. Ai, "A nonlinear control approach for a hypersonic vehicle," *Aircraft Engineering & Aerospace Technology*, vol. 89, no. 2, pp. 320–329, 2017.

[2] J. Xin and J. Jiang, "Design of adaptive switching control for hypersonic aircraft," *Advances in Mechanical Engineering*, vol. 7, no. 10, Article ID 168781401561046, 2015.

[3] B. Xu, S. Wang, D. Gao, Y. Zhang, and Z. Shi, "Command filter based robust nonlinear control of hypersonic aircraft with

magnitude constraints on states and actuators," *Journal of Intelligent & Robotic Systems*, vol. 73, no. 1-4, pp. 233–247, 2014.

[4] K. Hu, X. Wang, and C. Yang, "Hybrid adaptive dynamic inverse compensation for hypersonic vehicles with inertia uncertainty and disturbance," *Applied Sciences*, vol. 12, no. 21, p. 11032, 2022.

[5] B. Lyu, X. Yue, and C. Liu, "Constrained multi-observer-based fault-tolerant disturbance-rejection control for rigid spacecraft," *Internal Journal of Robust and Nonlinear Control*, vol. 34, no. 14, pp. 8102–8133, 2022.

[6] Y. Hu, Y. Yuan, H. Min, and F. C. Sun, "Multi-objective robust control based on fuzzy singularly perturbed models for hypersonic vehicles," *Science China: Information Sciences*, vol. 54, no. 3, pp. 563–576, 2011.

[7] X. Yan, G. Shao, Q. Yang, L. Yu, Y. Yao, and S. Tu, "Adaptive robust tracking control for near space vehicles with multi-source disturbances and input–output constraints," *Actuators*, vol. 11, no. 10, p. 273, 2022.

[8] C. Hu, X. Yang, X. Wei, and Y. Hu, "Robust model predictive control for hypersonic vehicle with state-dependent input constraints and parameter uncertainty," *International Journal of Robust and Nonlinear Control*, vol. 31, no. 18, pp. 9676–9691, 2021.

[9] K. An, Z. Y. Guo, W. Huang, and X. P. Xu, "Leap trajectory tracking control based on sliding mode theory for hypersonic gliding vehicle," *Journal of Zhejiang University-SCIENCE A*, vol. 23, no. 3, pp. 188–207, 2022.

[10] L. Chuang, Y. Xiaokui, Z. Jianqiao, and S. Keke, "Active disturbance rejection control for delayed electromagnetic docking of spacecraft in elliptical orbits," *IEEE Transactions on Aerospace and Electronic Systems*, vol. 58, no. 3, pp. 2257–2268, 2022.

[11] J. Shin, "Adaptive dynamic surface control for a hypersonic aircraft using neural networks," *IEEE Transactions on Aerospace and Electronic Systems*, vol. 53, no. 5, pp. 2277–2289, 2017.

[12] Y. Zhang, *Study of Nonlinear Methods for Longitudinal Control of Hypersonic Vehicles*, Huazhong University of Science and Technology, 2014.

[13] P. Cui, C. Gao, W. Jing, and R. An, "Fault-tolerant control of hypersonic vehicle using neural network and sliding mode," *International Journal of Aerospace Engineering*, vol. 2022, Article ID 1637305, 11 pages, 2022.

[14] H. Gao, W. Tang, and R. Fu, "Sliding mode control for hypersonic vehicle based on extreme learning machine neural network disturbance observer," *IEEE Access*, vol. 53, pp. 69333–69345, 2022.

[15] W. Chen, D. Ballance, and P. Gawthrop, "Optimal control of nonlinear systems: a predictive control approach," *Automatica*, vol. 39, no. 4, pp. 633–641, 2003.

[16] C. Hu, X. Wei, and Y. Ren, "Passive fault-tolerant control based on weighted LPV tube-MPC for air-breathing hypersonic vehicles," *International Journal of Control, Automation and Systems*, vol. 17, no. 8, pp. 1957–1970, 2019.

[17] K. Liu, Z. Hou, Z. She, and J. Guo, "Reentry attitude tracking control for hypersonic vehicle with reaction control systems via improved model predictive control approach," *Computer Modeling in Engineering and Sciences*, vol. 122, no. 1, pp. 131–148, 2020.

[18] S. Fesharaki, M. Kamali, F. Sheikholeslam, and H. A. Talebi, "Robust model predictive control with sliding mode for constrained non-linear systems," *IET Control Theory & Applications*, vol. 14, no. 17, pp. 2592–2599, 2020.

[19] C. Hu, X. Wei, L. Cao, Y. Tao, Z. Gao, and Y. Hu, "Integrated fault-tolerant control system design based on continuous model predictive control for longitudinal manoeuvre of hypersonic vehicle with actuator faults," *IET Control Theory & Applications*, vol. 14, no. 13, pp. 1769–1786, 2022.

[20] O. Li, J. Jiang, L. Deng, and S. Huang, "Anti-disturbance dynamic surface control for air-breathing hypersonic vehicles based on NDO," *Access*, vol. 10, pp. 76913–76925, 2022.

[21] N. Xiao, Y. Xiao, D. Ye, and Z. Sun, "Adaptive differential game for modular reconfigurable satellites based on neural network observer," *Aerospace Science and Technology*, vol. 128, article 107759, pp. 1–17, 2022.

[22] H. Zhao, X. Wu, Y. Xie, Y. du, Z. Zhang, and Y. Li, "Rotation matrix-based finite-time attitude synchronization control for flexible spacecrafts with unknown inertial parameters and actuator faults," *ISA Transactions*, vol. 128, pp. 276–289, 2022.

[23] Q. Wang and R. F. Stengel, "Robust nonlinear control of a hypersonic aircraft," *Journal of Guidance, Control and Dynamics*, vol. 23, no. 4, pp. 577–585, 2000.

[24] P. L. Moses, V. L. Rausch, L. T. Nguyen, and J. R. Hill, "NASA hypersonic flight demonstrators–overview, status, and future plans," *Acta Astronautica*, vol. 55, no. 3-9, pp. 619–630, 2004.

[25] P. Wang, *Research on Attitude Control Method for Hypersonic Cruise Vehicle*, Nation University of Defense Technology, 2013.

[26] P. Wang, L. Liu, and J. Wu, "The terminal sliding mode control system design for hypersonic flight vehicle," *Aerospace Control*, vol. 3, no. 5, pp. 9–14, 2012.

[27] K. Shi, C. Liu, Z. Sun, and X. Yue, "Coupled orbit-attitude dynamics and trajectory tracking control for spacecraft electromagnetic docking," *Applied Mathematical Modelling*, vol. 101, pp. 553–572, 2022.

[28] S. Wang, P. Guan, and X. Liu, "Nonlinear predictive control for hypersonic aircraft," *Journal of Beijing Information Science and Technology University*, vol. 28, no. 1, pp. 13–17, 2013.

[29] H. Rocha, "On the selection of the most adequate radial basis function," *Applied Mathematical Modelling*, vol. 33, no. 3, pp. 1573–1583, 2009.

[30] Y. Abe and Y. Iiguni, "Fast computation of RBF coefficients using FFT," *Signal Processing*, vol. 86, no. 11, pp. 3264–3274, 2006.

[31] L. Fei, C. Yang, and J. Qiao, "A novel RBF neural network design based on immune algorithm system," in *2017 36th Chinese Control Conference (CCC). IEEE*, pp. 4598–4603, Dalian, China, July 2017.

[32] A. Isidori, *Nonlinear Control Systems: An Introduction*, Springer-Verlag World Publishing Corp, 1995.

[33] X. Tan, J. Yi, D. Zhao, and Y. Hao, "Simulation research on tracking control for hypersonic aircraft," *Journal of System Simulation*, vol. 23, no. 4, pp. 745–749, 2011.

[34] H. Xu, M. D. Mirmirani, and P. Ioannou, "Adaptive sliding mode control design for a hypersonic flight vehicle," *Journal of Guidance, Control, and Dynamics*, vol. 27, no. 5, pp. 829–838, 2004.